Supplementary Information for "Improved superconducting qubit state readout by path interference"

Zhiling Wang,* Zenghui Bao,* Yukai Wu, Yan Li, Cheng Ma,
Tianqi Cai, Yipu Song, Hongyi Zhang,† and Luming Duan‡
Center for Quantum Information, Institute for Interdisciplinary Information Sciences, Tsinghua University, Beijing 100084, PR China

(Dated: October 15, 2021)

*These two authors contributed equally to this work.
†Electronic address: hyzhang2016@tsinghua.edu.cn
‡Electronic address: lmduan@tsinghua.edu.cn

I. THEORY

For a superconducting qubit dispersively coupled to a cavity, the Hamiltonian of the system can be written as $H = (\omega_r + \chi\sigma_z)a^\dagger a + \omega_q\sigma_z/2$, which means the resonant frequency of the cavity depends on the state of the qubit. The photon state in the readout cavity can be calculated from the evolution of annihilation operator,

$$\frac{\partial\alpha}{\partial t} = -i(\omega_d - (\omega_r + \chi\sigma_z))\alpha - \frac{\kappa}{2}\alpha + \sqrt{\kappa_c/2}\alpha_{in} \tag{S1}$$

where κ_c is the damping rate of the cavity to the transmission line and $\kappa = \kappa_c + \kappa_i$ is the total damping rate, with κ_i being the internal damping rate of the cavity. ω_d is the frequency of the probe field and α_{in} represents the strength of the probe field. From Eq. (S1), the steady state in the readout cavity can be written as $\alpha = \frac{\sqrt{\kappa_c/2}\alpha_{in}}{i(\omega_d-(\omega_r+\chi\sigma_z))+\kappa/2}$. According to the input-output theory, photon states of transmission and reflection from the hanger cavity can be written as

$$\begin{aligned}
\alpha_T(\omega_d,\sigma_z) &= \alpha_{in} - \sqrt{\kappa_c/2}\alpha \\
&= (1 - \frac{\kappa_c/\kappa}{1 + 2i(\omega_d - \omega_r - \chi\sigma_z)/\kappa})\alpha_{in}, \\
\alpha_R(\omega_d,\sigma_z) &= -\sqrt{\kappa_c/2}\alpha \\
&= -\frac{\kappa_c/\kappa}{1 + 2i(\omega_d - \omega_r - \chi\sigma_z)/\kappa}\alpha_{in}
\end{aligned} \tag{S2}$$

Therefore, for a given qubit state, when sweeping the probe frequency the measured cavity response would be a circle on the phase plane, which is referred to IQ circle in the following context. Examples can be found in Fig. 2(b) in the main text.

For a given probe frequency, the distance between the two pointer states corresponding to the qubit states $|g\rangle$ and $|e\rangle$ from T and R would be

$$\begin{aligned}
D_{ge}^T &= |\alpha_T(\omega_d, 1) - \alpha_T(\omega_d, -1)| \\
&= \frac{4\kappa_c\chi|\alpha_{in}|}{\sqrt{(\kappa^2 + 4\chi^2 - 4(\omega_d - \omega_r)^2)^2 + 16\kappa^2(\omega_d - \omega_r)^2}} \\
D_{ge}^R &= |\alpha_R(\omega_d, 1) - \alpha_R(\omega_d, -1)| \\
&= \frac{4\kappa_c\chi|\alpha_{in}|}{\sqrt{(\kappa^2 + 4\chi^2 - 4(\omega_d - \omega_r)^2)^2 + 16\kappa^2(\omega_d - \omega_r)^2}}
\end{aligned} \tag{S3}$$

From Eq. (S3), one can see that the distance between the two pointer states are equal, as a result of the symmetrical coupling of the hanger cavity.

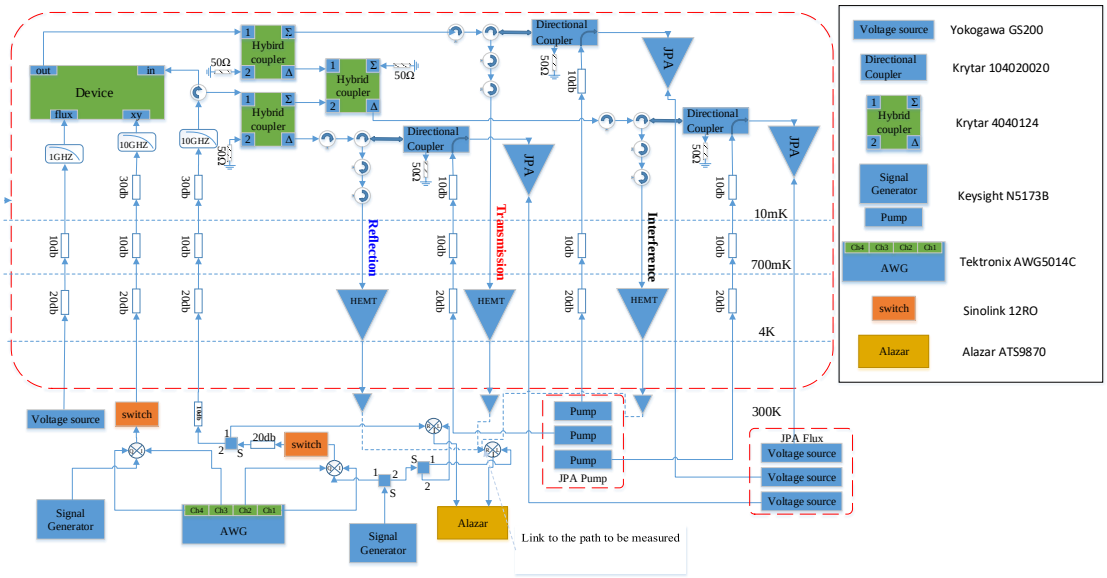

FIG. S1: Schematic of the experimental setup.

In order to effectively collect the cavity photons, we use a beam splitter to combine transmission and reflection signals, generating interference signals labeled as plus mode and minus mode,

$$\alpha^{int}(\omega_d, \sigma_z) = \frac{\alpha_T(\omega_d, \sigma_z) \pm e^{i\theta_{RT}} \alpha_R(\omega_d, \sigma_z)}{\sqrt{2}} \tag{S4}$$

where θ_{RT} characterizes the phase difference between transmission mode and reflection mode, due to the imbalanced circuit lengths when they are interfered at the beam splitter. θ_{RT} can be measured in the experiment. The distance between the two pointer states for the interference output would be

$$\begin{aligned} D_{ge}^{int}(\theta) &= |\alpha_{int}(\omega_d, 1) \pm \alpha_{int}(\omega_d, -1)| \\ &= \left| \frac{1 \pm e^{i\theta_{rt}}}{\sqrt{2}} \right| \frac{4\kappa_c \chi |\alpha_{in}|}{\sqrt{(\kappa^2 + 4\chi^2 - 4(\omega_d - \omega_r)^2)^2 + 16\kappa^2(\omega_d - \omega_r)^2}} \end{aligned} \tag{S5}$$

One can see that the distance between the two pointer states from interference output can be maximally enlarged by a factor of $\sqrt{2}$ compared with that from either transmission or reflection, as illustrated in inset of Fig. 3 in the main text.

As mentioned in Fig. 2(b) of the main text, IQ circle of the excited state is smaller than that of the ground state, which can be explained by a finite qubit energy relaxation time T_1 of the qubit. The diameter of the IQ circle can be estimated based on Eq. (S2) by taking

ω_d as the cavity resonance or a value far off the cavity resonance. The resulting distance reads $d_g = \alpha_{in}\kappa_c/\kappa$. For a finite T_1, the measured cavity response when the qubit is in $|e\rangle$ is partially mixed with that when the qubit is in $|g\rangle$, and the resulting diameter (normalized to the input state) of the IQ circle can be written as

$$d_e/\alpha_{in} = \kappa_c/\kappa \left| 1 - \exp\left(-\frac{t_m}{2T_1}\right) + \exp\left(-\frac{t_m}{2T_1}\right)\exp(i\delta) \right| \tag{S6}$$

where δ is the phase shift of the cavity response when the qubit is excited from $|g\rangle$ to $|e\rangle$, which is about $4\chi/\kappa$. The exponential factor originates from the qubit energy relaxation. It is clear that d_e will be smaller than d_g, which explains the difference between Fig. 2(b) and inset of Fig. 2(b) in the main text.

II. EXPERIMENTAL SETUP

Fig. 2(a) in the main text is a schematic of our sample and a part of the measurement setup. The sample is made from an aluminum film on a 7 mm×7 mm sapphire substrate. The Josephson junction of the transmon qubit is made by Al/AlO_x/Al. We use a hanger type cavity dispersively coupled to the qubit for state readout. The sample is wire bonded onto a PCB board in an aluminium sample box and cooled to about 14 mK by a dilution refrigerator. The measurement setup is illustrated in Fig. S1. Details about the device parameters are listed in Table S1. In particular, as shown in Fig. S1, three Josephson parametric amplifiers (JPA) are used in the single shot qubit state measurement, for which signal gains of 20 dB, 14 dB and 21 dB for transmission, reflection and interference outputs, respectively. The JPAs are not used during the steady state spectral measurements for the cavities.

Transmission and reflection are interfered with a hybrid coupler (Krytar 4040124) as illustrated in Fig. S1. In order to keep the off-chip optical lengths for T and R as close as possible, we use three 15 inch RF cables and four SMA connectors/adapters to connect the chip with the interfering hybrid coupler for both T and R. In order to realize varied θ_{RT} for different qubits, the readout cavity for each qubit is equally spaced by about $l = 2.5$ mm along the transmission line, which naturally serves as a path difference of $2l$ between the signals through T and R. In the experiments we will also measure θ_{RT} for each qubit, as discussed in Appendix III. It worth noting that for the purpose of applying the proposed

TABLE S1: device parameters

	Q1	Q2	Q3	Q4	Q5
$\omega_r/2\pi$(GHz)	7.9224	7.9756	8.1237	8.1366	8.1460
Q_i	8350	10502	8794	8391	2580
Q_c	6821	5704	7044	3846	3289
ω_q(GHz)	5.938	5.642	6.067	5.933	5.313
$\chi/2\pi$(MHz)	-0.4	-0.25	-0.35	-0.4	-0.35
$T_1(\mu s)$	2.40	1.82	1.19	3.24	8.92
θ_{RT}	-1.42	0.11	0.70	1.82	2.60

scheme to realize simultaneous improvement for multiple cavities coupled to a common transmission line, the cavity spacing can be set to half of the wavelength corresponding to the mean resonance frequency of the cavities, and a cryogenic phase shifter is required to compensate the global relative phase difference induced by the possible imbalanced optical path between reflection and transmission.

The amplification factors of the three output lines have to be carefully calibrated before making comparison among output T, R and $T+R$. In principle it can be done by counting attenuation and amplification factors of all microwave elements on the three output lines. But in practice it would be tricky to achieve a high accuracy calibration in this way, since the calibrations have to be done at room temperature but the experiments are carried out at cryogenic temperature. Therefore, we perform the calibration by comparing spectra measured from the three outputs.

In Fig. 2(a), after hybrid couplers the photon states from T, R and $T+R$ can be related as

$$a_0^+ = a_0^T + a_0^R \tag{S7}$$

As illustrated in Fig. S1, after passing HEMT, room temperature amplifiers and other microwave elements, the photon states get amplified and acquire an additional phase. The corresponding photon state can be written as $A^T = c^T a_0^T$, $A^R = c^R a_0^R$ and $A^+ = c^+ a_0^+$, where c^T, c^R and c^+ represent the correspondingly amplification factors of each output line. The amplified state can be measured with a vector network analyzer. From Eq. (S7) we

have

$$A^+ = \frac{c^+}{c^T}A^T + \frac{c^+}{c^R}A^R, \tag{S8}$$

which relates the three amplified state. The corresponding amplification factors can be obtained by spectra fitting according to Eq. (S8), and thus the three outputs can be compared through the calibrated amplification factors.

III. CALIBRATE THE RELATIVE PHASE

As indicated in Eq. (3) in the main text, the relative phase θ_{RT} is a critical parameter to characterize the readout enhancement. θ_{RT} is related to the circuit length and microwave elements before the hybrid coupler, thus it is difficult to be determined directly.

In this part we describe an effective approach to determine θ_{RT} for each qubit. We send a microwave probe at the frequency $\omega_r - \chi$ with an average photon number of N, which is on resonance with the cavity when the qubit is at the ground state $|g\rangle$. Due to the conservation of energy, we get following equations

$$\begin{aligned} |\alpha_g^T|^2 + |\alpha_g^R|^2 &= r_g N, \\ |\alpha_e^T|^2 + |\alpha_e^R|^2 &= r_e N, \end{aligned} \tag{S9}$$

where the factor 1-r_g or 1-r_e is the internal loss introduced by the cavity when the qubit is at $|g\rangle$ or $|e\rangle$, which can be obtained from the spectra of the cavity. Theoretically they are given as

$$\begin{aligned} r_g &= \left|\frac{\alpha_T(\omega_r - \chi, -1)}{\alpha_{in}}\right|^2 + \left|\frac{\alpha_T(\omega_r - \chi, -1)}{\alpha_{in}}\right|^2 \\ &= \frac{\kappa_c^2 + \kappa_i^2}{(\kappa_c + \kappa_i)^2} \\ r_e &= \left|\frac{\alpha_T(\omega_r - \chi, 1)}{\alpha_{in}}\right|^2 + \left|\frac{\alpha_T(\omega_r - \chi, 1)}{\alpha_{in}}\right|^2 \\ &= 1 - \frac{2\kappa_c\kappa_i}{(\kappa_c + \kappa_i)^2 + 16\chi^2} \end{aligned} \tag{S10}$$

In order to avoid comparisons among different output lines, we focus on the same output line but different qubit states. Comparing the photon states when the qubit is at $|g\rangle$ and

$|e\rangle$ for either T and R, one would have

$$\begin{aligned}\gamma_T &= \alpha_e^T/\alpha_g^T,\\ \gamma_R &= \alpha_g^R/\alpha_e^R\end{aligned} \tag{S11}$$

where γ_T and γ_R are complex numbers which contain both the amplitude and phase information. They can be measured in the experiment by comparing the output signals when the qubit is set to $|g\rangle$ and $|e\rangle$, for either of the output line T or R.

Solving Eq. (S10) and Eq. (S11), the photon states can be written as

$$\begin{aligned}\alpha_g^T &= \sqrt{N}\sqrt{\frac{r_g - r_e|\gamma_R|^2}{1-|\gamma_T\gamma_R|^2}},\\ \alpha_e^T &= \gamma_T\sqrt{N}\sqrt{\frac{r_g - r_e|\gamma_R|^2}{1-|\gamma_T\gamma_R|^2}},\\ \alpha_g^R &= \gamma_R\sqrt{N}\sqrt{\frac{r_e - r_g|\gamma_T|^2}{1-|\gamma_T\gamma_R|^2}},\\ \alpha_e^R &= \sqrt{N}\sqrt{\frac{r_e - r_g|\gamma_T|^2}{1-|\gamma_T\gamma_R|^2}}\end{aligned} \tag{S12}$$

Two of the relative phases among these four complex amplitudes are fixed by γ_T and γ_R, and the remaining one can be absorbed into θ_{RT} in Eq. (S4) after interference.

Taking Eq. (S12) into Eq. (S4) we have

$$\begin{aligned}\alpha_g^+ &= \frac{\alpha_g^T + e^{i\theta_{RT}}\alpha_g^R}{\sqrt{2}}\\ &= \sqrt{\frac{N}{2}}\left(\sqrt{\frac{r_g - r_e|\gamma_R|^2}{1-|\gamma_T\gamma_R|^2}} + \gamma_R e^{i\theta_{RT}}\sqrt{\frac{r_e - r_g|\gamma_T|^2}{1-|\gamma_T\gamma_R|^2}}\right),\\ \alpha_e^+ &= \frac{\alpha_e^T + e^{i\theta_{RT}}\alpha_e^R}{\sqrt{2}}\\ &= \sqrt{\frac{N}{2}}\left(\gamma_T\sqrt{\frac{r_g - r_e|\gamma_R|^2}{1-|\gamma_T\gamma_R|^2}} + e^{i\theta_{RT}}\sqrt{\frac{r_e - r_g|\gamma_T|^2}{1-|\gamma_T\gamma_R|^2}}\right).\end{aligned} \tag{S13}$$

The amplitude ratio of the interference signal $\gamma_+ = \alpha_e^+/\alpha_g^+$ can also be measured in the experiment. The expression of θ_{RT} can be deduced based on Eq. (S4) and Eq. (S12), which reads as

$$\exp(i\theta_{RT}) = \frac{\alpha_e^T - \gamma_+\alpha_g^T}{\gamma_+\alpha_g^R - \alpha_e^R} = \frac{(-\gamma_+ + \gamma_T)\sqrt{r_g - r_e|\gamma_R|^2}}{(-1+\gamma_+\gamma_R)\sqrt{r_e - r_g|\gamma_T|^2}}. \tag{S14}$$

In the experiment, we first set the qubit in either $|g\rangle$ or $|e\rangle$, then send the cavity probe signal at frequency $\omega_r - \chi$ with certain average photon numbers. On the output line of T, R

and $T+R$, the photon states $\alpha_{0(1)}^{T}$, $\alpha_{0(1)}^{R}$ and $\alpha_{0(1)}^{+}$ can be measured, from which γ_R , γ_T and γ_+ can be deduced from their definitions. All of the measurements are repeated for 40 times to reduce statistical errors. Then the value of θ_{RT} can be calculated based on Eq. (S14). The results are shown in the inset of Fig. 3 of the main text as the horizontal axis.

IV. SINGLE SHOT MEASUREMENT

In the single shot experiment we compare histogram plots of the measured cavity response and the resulting fidelity when measuring from output T and output $T+R$. Since the amplification and detection efficiency of the two output circuits are not necessarily the same, we have to first calibrate the circuit parameters before the comparison. In the measurement setup we use homodyne detection to map the amplified output photon state to the voltages, therefore $\langle\alpha\rangle$ and the variance of measured photon state is mapped as the mean value and the variance of the measured voltage distribution. For a coherent state input readout signal, the output signal can be regarded as a coherent state convoluted with the added noise from the amplification chain. This added noise does not change the mean value of the measured voltage, but it broadens the voltage distribution and thus leads to a larger variance σ_m [1]. Here we can define the circuit efficiency $\eta = 1/(1+N_0)$ to describe the added noise N_0. It has been shown that the noisy variance σ_m and the original variance σ_0 are related as $\sigma_m = \sigma_0/\sqrt{\eta}$ [2].

The circuit efficiency can be calibrated by measuring the variance of voltage distribution with different measurement time t_m. Using the fitting model $\sigma_m = c_0/\sqrt{t_m}$, we can get the parameter c_0 which is proportional to $1/\sqrt{\eta}$ [2]. The corresponding measurement data and fitting results for output T circuit and $T+R$ circuit are shown in Fig. S2. We get $c_0^{T+R} = 0.3598 \pm 0.0008$ and $c_0^{T} = 0.3915 \pm 0.0006$ respectively, with the ratio of the circuit efficiencies $\eta_{T+R}/\eta_T = (c_0^T/c_0^{T+R})^2 = 1.1838$. When comparing the measurement results between T and $T+R$, the variance of the histogram result for $T+R$ output σ_{T+R} is rescaled as $\sigma'_{T+R} = c_0^T/c_0^{T+R}\sigma_{T+R}$ to remove the efficiency difference between two output circuits. After this process, Fig. 4(c) in the main text can be obtained.

Now we discuss the potential of reducing the total readout error when using path interference compared with using simply transmission or reflection. As mentioned in the main text, the total readout error can be written as the sum of measurement error, qubit relax-

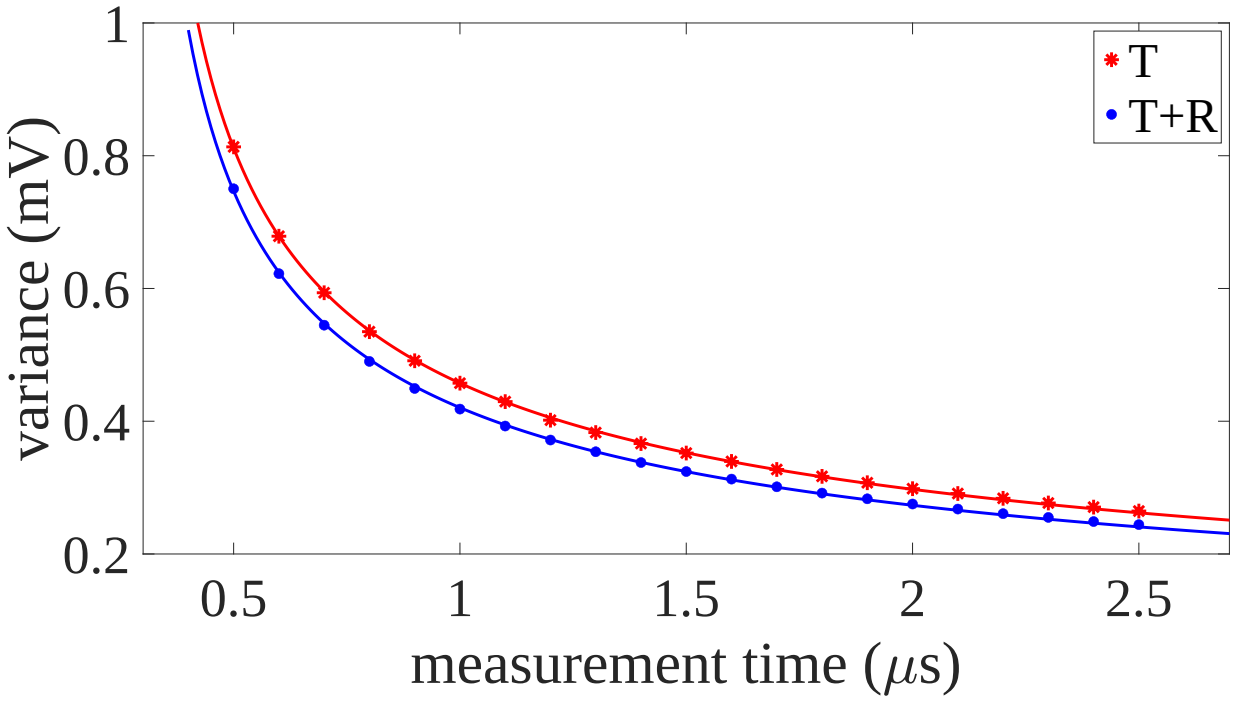

FIG. S2: The variance of the readout signal as a function of measurement time for different circuits. The blue (red) scattered plots are experimental data from output T ($T+R$), and the lines are the corresponding fitting results.

ation induced error and thermal population induced error, The thermal population induced error P_{th} can be estimated via the Boltzmann distribution, $\frac{\exp(-\hbar\omega_q/k_bT_e)}{1+\exp(-\hbar\omega_q/k_bT_e)}$ [3], where T_e is the device temperature. The thermal population induced error can be greatly suppressed by improving the thermal anchoring of the sample and coaxial cables and using carefully selected filters and attenuators [4], which we will not discuss here.

The measurement error P_m can be expressed in terms of measurement time t_m and distance D between two pointer states corresponding to the two qubit states, $P_m = 1 - \mathrm{Erf}(\sqrt{\eta t_m}D/\sqrt{2})$ [2]. The distance of the pointer states D is related to the cavity photon number n_c as $D^T = \frac{\sqrt{2\kappa_c n_c}}{\sqrt{1+(\frac{\kappa}{2\chi})^2}}$, where we take the distance on the output T D_T as an example. Neglecting the thermal population induced error, we have

$$\begin{aligned} P_{err} &\sim P_m + P_{T_1} \\ &= 1 - \exp\left(-\frac{t_m}{2T_1}\right) + 1 - \mathrm{Erf}(\sqrt{\eta t_m}D/\sqrt{2}). \end{aligned} \tag{S15}$$

From Eq. (S15), a longer measurement time is preferred to reduce the measurement error, but on the other hand will increase the qubit relaxation induced error. We can define an optimized measurement time $t_{optimal}$ which yields the minimum total readout error. By taking the derivative of Eq. (S15), $t_{optimal}$ can be obtained as

$$t_{optimal} = \frac{T_1}{\eta D^2 T_1 - 1} \mathrm{W}(\frac{2\eta D^2 T_1}{\pi}(\eta D^2 T_1 - 1)), \tag{S16}$$

where W is Lambert W function. The minimum qubit readout error $P_{err}^{min}(T_1, D)$ can be obtained by plug $t_{optimal}$ back into Eq. (S15). As a specific example, we take the circuit efficiency $\eta = 0.25$, the cavity photon number $n_c = 20$, the device temperature $T_e \sim 20\,\mathrm{mK}$, and the qubit frequency $\omega_q \sim 6\,\mathrm{GHz}$ based on our measurement circuit. Then the total readout error with the optimized measurement time for T and $T+R$ outputs can be obtained according to Eq. (S15) and Eq. (S16). The corresponding results are shown in Fig. 4(d) of the main text.

---

[1] C. Eichler, Ph.D. thesis, ETH Zurich, Zurich (2013).

[2] E. A. Sete, J. M. Martinis, and A. N. Korotkov, Physical Review A **92**, 012325 (2015).

[3] P. Krantz, A. Bengtsson, M. Simoen, S. Gustavsson, V. Shumeiko, W. D. Oliver, C. M. Wilson, P. Delsing, and J. Bylander, Nature Communications **7**, 11417 (2016), ISSN 2041-1723.

[4] S. Krinner, S. Storz, P. Kurpiers, P. Magnard, J. Heinsoo, R. Keller, J. Lütolf, C. Eichler, and A. Wallraff, EPJ Quantum Technology **6**, 2 (2019), ISSN 2196-0763.